Stability Augmentation and Control Decoupling for the Airborne Remotely Operated Device

John E. White* and John R. Phelan†
Sandia National Laboratories, Albuquerque, New Mexico 87185

A control system for the Marine Corps Airborne Remotely Operated Device is described. This unmanned air vehicle is designed to provide frontline Marines with a portable, short range, aerial reconaissance capability. The chosen configuration has a single gasoline engine and propellor enclosed in an airfoil shroud with four aerodynamic control surfaces located just aft of the shroud. The control system is designed to provide stability augmentation so that a Marine with minimal training will be able to fly the vehicle. One interesting aspect of the control problem is the gyroscopic coupling between two of the control channels due to the single propellor design. The multi-input/multi-output nature of this problem has been the motivation for the use of a linear-quadratic-regulator controller synthesis technique. Simulation time responses and a singular value analysis are employed to assess the performance of the control system. A limited flight test program has also been used to evaluate performance.

I. Introduction

SANDIA National Laboratories has recently completed development of a ducted-propellor unmanned air vehicle for the Marine Corps, which is designed to be teleoperated by frontline marines to provide an "over-the-next-hill" reconnaissance capability. This vehicle has been named the Airborne Remotely Operated Device (AROD) and is depicted in Fig. 1. The focus of the AROD program is the development of a camera platform that can hover, fly at speeds up to 30 kt in still air, and takeoff and land vertically. Onboard cameras, directed by the operator, provide realtime surveillance images for transmission back to an operator station via a fiber optic link. A radio frequency link is available for backup control communications purposes. The maximum intended range for AROD is about 2 km with 5 km of fiber optic cable available during a typical flight. Maximum flight time is 1 h. Portability requirements restrict the size and weight of the flight vehicle and the support equipment.

AROD is intended to be flown by an average marine with minimal training. Operational requirements dictate that the vehicle be teleoperated, and a control scheme employing a preprogrammed, handsoff autopilot has not been considered. Instead, the control system is designed to provide stability augmentation and decoupled control axes, such that AROD can be flown safely and logically by an individual with minimum training.

The Sandia AROD vehicle, although independently conceived, is similar in configuration to a General Dynamics-Convair Division design that was developed in 1976. Recent attempts to provide similar vertical takeoff and landing airborne surveillance capabilities include the Canadair "Peanut" and the M.L. Aviation "Sprite." Both of these vehicles have unshrouded, counter-rotating propellors. The counter-rotating propellors eliminate the control problems associated with gyroscopic coupling, at the expense of increased mechanical complexity.

The organization of this paper is as follows. Section II discusses the design approach and includes comments regarding the important system issues such as sensors, servos, aerodynamics, and dynamic coupling. The assumptions upon which the control-system design is predicated are also described. Section III discusses the linear dynamic model upon which the control system is based. Section IV defines the compensator structures, and Sec. V describes the determination of gains. Section VI discusses the singular value procedures used to evaluate controller gain and phase margins and robustness to parameter uncertainty. Section VII discusses simulation results and the development test program.

Presented as Paper 87-2453 at the AIAA Guidance, Navigation, and Control Conference, Monterey, CA, Aug. 17-19, 1987; received April 4, 1989; revision received July 31, 1989.

*Senior Member of Technical Staff. Member AIAA.
†Distinguished Member of Technical Staff. Member AIAA.

II. AROD Control Design Issues

The mission requirements stated in Sec. I have shaped the AROD development process. General information on the AROD design can be found in Ref. 1. The remainder of this section will discuss those issues that directly influence the design and operation of the AROD control system.

A. Control Objectives

The teleoperation requirement for AROD has led to constraints on the control-system operation. Specifically, an early requirement called for control of vertical and horizontal velocities and rotation rates. Hence, the operator-commanded variables are chosen as rate of climb, roll rate, pitch angle, and yaw angle. A capability to command engine speed is also required for preflight checkout tests. The body fixed axes are defined in Fig. 1, where roll is about the x axis, pitch is about the y axis, and yaw is about the z axis. The steady-state horizontal velocity of the AROD configuration is directly related to the vehicle attitude, and commands of pitch and yaw angle are interpreted by the operator as velocity commands. Roll-rate control is useful at hover to slew the cameras, but roll-angle control is probably more appropriate for translational flight. Some tests with roll-angle control were conducted late in the development program.

B. Hardware Considerations

The hardware with direct impact on the control system include the flight computer, control servos, and sensors. The flight computer selected is based on a 68000 processor with 64 K bytes of random access memory. The number of functions handled by the flight computer has increased to the point that the sample rate has decreased to 8 times/s with a corresponding computation delay of 0.12 s. Software optimization and/or a more capable flight computer are likely candidate projects for any future development efforts.

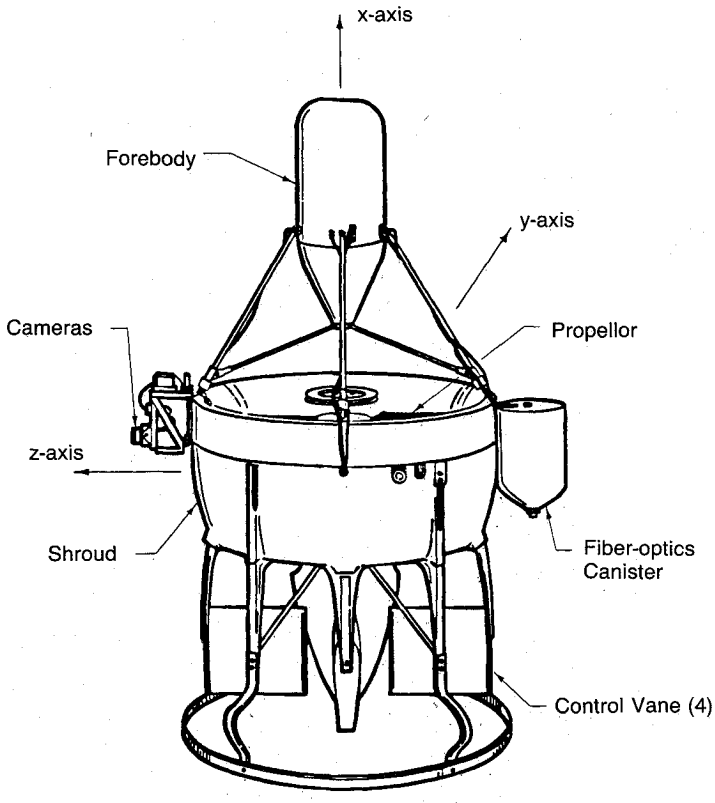

Fig. 1 AROD schematic and axes definition.

The control servos incorporated into AROD are off-the-shelf, position-commanded, quarter-scale model airplane servos. These servos are lightweight and very low cost, although their natural frequency (about 3.2 Hz) has been a limiting factor on the control-system bandwidth. Five of these servos are used on AROD, four to drive the aerodynamic control surfaces and one to drive the engine throttle. The control-law outputs must first be blended to properly command the four control-vane servos.

The sensor package includes a barometric altimeter, a vertical gyro, a 3-axis fluxgate magnetometer, and rate gyros and accelerometers in all three axes. Because the airflow around AROD is complex and varies considerably with the flight mode, no air-relative velocity or angle-of-attack sensors have been used in the current sensor package. The available sensors are used to provide feedbacks to the control system. The altimeter provides an altitude measurement and is also used with accelerometer data to estimate the altitude-rate state. The vertical gyro provides feedback on pitch and yaw angles. The magnetometer is used to provide heading angle data. Magnetometer and accelerometer outputs are both processed with vertical gyro data to compensate for changes in vehicle attitude. The rate gyros provide pitch-, yaw-, and roll-rate feedbacks.

C. Dynamic Coupling

Because of the nature of the AROD configuration, the dynamic behavior about a given axis is coupled with other vehicle dynamics. In particular, there are three types of coupling to be evaluated for AROD. The single propellor design introduces a gyroscopic coupling between the pitch and yaw axes. The relative importance of this coupling is a function of the inertia and angular velocity of the rotating component(s). For the existing AROD design, active control must be used to decouple the pitch and yaw axes. Simulation experience and field tests with AROD mounted in a gimballed fixture have demonstrated that unstable behavior will result if single-axis control is attempted. Simulations have also shown that the multi-input/multi-output (MIMO) nature of a linear-quadratic-regulator (LQR) design process produces better decoupling than a typical classical approach of designing two independent single-input/single-output (SISO) loops and then connecting those loops with dynamically intuitive crossover paths. The performance of the classical approach improves as the servo natural frequency is increased with other system parameters held fixed. The difficulty of the decoupling problem is, therefore, also a function of the performance of the control servos.

A second dynamic coupling exists between the altitude-rate control loop and the vehicle attitude, since a loss of lift due to thrust occurs when the vehicle is tilted to generate horizontal motion. Wind-tunnel test data indicate, however, that an aerodynamic lift force is generated in steady-state horizontal flight, which approximately replaces the loss of thrust lift for the range of attitudes of interest. This coupling is ignored during the compensator design process, although actual implementation includes a bias on the engine speed command that is a function of the vehicle attitude. This mechanization is intended to reduce the loss of altitude during the transition between steady-state flight conditions.

The third dynamic coupling exists between the altitude and roll control loops due to the reactive torques applied to the roll axis as the engine speed is varied. The current control system ignores this coupling and relies on the integrator in the roll-rate loop to maintain steady-state tracking. This decision is based on wind-tunnel data that suggest that large engine speed changes are not required during flight.

Table 1 AROD wind-tunnel test data

Control-vane effectiveness data	
Vane deflection, deg	Pitch moment, ft-lb
0	0
+10	−6.8
+15	−9.7
+20	−13.5

Trim flight conditions			
Angle of attack, deg	Velocity, ft/s	Control-vane deflection, deg	Pitch moment, ft-lb
80	12.98	+6.6	+4.5
75	15.02	+9.7	+6.5
70	23.05	+10.8	+7.3
65	28.55	+11.0	+7.5
60	35.16	+7.9	+5.4
55	40.92	+7.7	+5.2
50	48.68	+5.9	+4.1

D. Aerodynamics

A wind-tunnel test program has been used to evaluate the aerodynamics of the AROD configuration.[2] Table 1 gives the control torques available from two control surfaces at a hover flight condition with a center of gravity located at 4.5 in. aft of the shroud leading edge. The control-vane effectiveness (slope) is approximately constant out to at least 25 deg of deflection. These data have been verified in gimbal fixture field tests. Wind-tunnel data also indicate that the control-surface effectiveness is about the same for translational flight as that at hover. The control vanes are located in the high-speed flow aft of the propellor and their effectiveness is not appreciably affected by the freestream crossflow.

Table 1 also gives the steady-state translational velocities and aerodynamic pitching moments for several angles of attack. The pitching-moment data suggest that the angle-of-attack aerodynamics are stabilizing out to a 70-deg angle of attack and somewhat destabilizing for angles of attack between 70 and 50 deg. These aerodynamics have been neglected in the current control design. Simulation studies indicate that

all mission objectives can be met with adequate performance with this design approach. This assumption also simplifies the controller implementation. Section III will show that a single set of gains can then be used for all flight modes.

The data of Table 1 also show that the 30 kt velocity requirement will require level flight with about 40 deg of pitch away from hover. Data similar to that shown in Table 1, but for other center-of-gravity (c.g.) locations, indicate that trim control-surface deflections can be maintained at 15 deg or less only if the c.g. is no further than 5 in. aft of the duct leading edge. Power data taken during the wind-tunnel test, although noisy, indicate that steady-state engine power requirements are relatively constant from hover out to 40 deg of pitch because aerodynamic lift forces replace the loss of thrust lift as the vehicle achieves level flight.

III. Linear System Dynamics

The AROD control-system design is based on a simple linear dynamic model that uses hover as the equilibrium flight condition. This model is also acceptable as an approximation of the translational dynamics because the control-surface and engine effectiveness parameters and the nominal engine rpm, are relatively constant for the flight modes of interest. All aerodynamic coefficients have been neglected in this model except for the control-vane effectiveness parameters. The linear equations of motion are

$$\dot{\theta} = \int \dot{q}\, dt \tag{1}$$

$$\dot{q} = M_r r + M_E \delta_E \tag{2}$$

$$\dot{\psi} = \int \dot{r}\, dt \tag{3}$$

$$\dot{r} = N_q q + N_R \delta_R \tag{4}$$

$$\dot{p} = L_A \delta_A \tag{5}$$

$$\ddot{h} = [(X_{\text{rpm}}/W)(C_{\text{rpm}})]\Omega \tag{6}$$

where terms such as M_q, M_θ, N_r, N_ψ, and L_p have been neglected. None of these terms are available from wind-tunnel test data. The terms M_q, N_r, and L_p are expected to be stabilizing, and their omission should not adversely affect control-system performance. The terms M_θ and N_ψ are assumed to be small, despite being functions of the gravity vector. These coefficients are also functions of moment vs angle-of-attack-rate stability derivatives that are expected to be very small for the AROD configuration, especially since the control surfaces are embedded in the high-speed flow downstream of the propellor. The system parameters are defined by

$$M_r = -(I_P \omega_P / B), \qquad N_q = (I_P \omega_P / C)$$

where I_P is the propellor moment of inertia about the x axis; ω_P the propellor hover rotation rate; B and C the moments of inertia (including propellor) about the y and z axes; W the vehicle weight; M_E, N_R, L_A the pitch-, yaw-, and roll-vane effectiveness coefficients; X_{rpm} the slope of the thrust vs engine rpm curve at hover; and $C_{\text{rpm}} = (2\pi)(32.2/60)$. The perturbed states are defined as pitch angle θ; pitch rate q; yaw angle ψ; yaw rate r; roll rate p; altitude h; change in engine rpm from the nominal hover rpm, Ω; and pitch-, yaw-, and roll-vane deflection angles, δ_E, δ_R, and δ_A. The gyroscopic coupling between the pitch and yaw axes is evident from Eqs. (2) and (4).

The control servos can be modeled as second-order systems with a natural frequency of f_n and damping ratio of £. The differential equations are

$$\dot{\delta}_i = \int \ddot{\delta}_i\, dt \tag{7}$$

$$\ddot{\delta}_i = -H_1 \dot{\delta}_i - H_2 \delta_i + H_2 u_i \tag{8}$$

where i is replaced by E, R, A, or T depending on which servo is being discussed, and u_i represents the position control input to the respective servo. The coefficients are defined by $H_1 = 2£f_n$ and $H_2 = f_n^2$.

The two-cycle, two-cylinder gasoline engine is similarly modeled as

$$\dot{\Sigma} = \int \ddot{\Sigma}\, dt \tag{9}$$

$$\ddot{\Sigma} = -H_{E1}\dot{\Sigma} - H_{E2}\Sigma + H_{E2} K_E \delta_T \tag{10}$$

where K_E is a scale factor, δ_T the throttle servo position angle, and Σ the engine speed in revolutions per minute. The coefficients in Eq. (10) are defined analogous to those of Eq. (8).

IV. State Space Construction

The section will construct state spaces that are compatible with LQR synthesis. These state spaces define the AROD compensator structures.

The system tracking errors are natural state variables for the LQR synthesis procedure.[3,4] The tracking errors in the AROD design are

$$E_\theta = \theta_C - \theta \tag{11}$$

$$E_\psi = \psi_C - \psi \tag{12}$$

$$E_p = p_C - p \tag{13}$$

$$E_{\dot{h}} = \dot{h}_C - \dot{h} \tag{14}$$

$$E_\Sigma = \Sigma_C - \Sigma \tag{15}$$

where the variables with C subscripts are step input commands from the control stick, and the state variables without subscripts are measured or estimated feedbacks. The differential equations for the tracking errors are

$$\dot{E}_\theta = -q \tag{16}$$

$$\dot{E}_\psi = -r \tag{17}$$

$$\dot{E}_p = -\dot{p} \tag{18}$$

$$\dot{E}_{\dot{h}} = -\ddot{h} \tag{19}$$

$$\dot{E}_\Sigma = -\dot{\Sigma} \tag{20}$$

A state space for the MIMO pitch- and yaw-angle control problem can be constructed by combining Eqs. (16) and (17) with Eqs. (1–4), (7), and (8) to form a consistent state space. All of the state variables (e.g., δ_E and δ_R) do not generally have zero steady-state values. Hence, each of these equations is differentiated and combined with Eqs. (16) and (17) to form a new state space that is consistent, controllable, has no input command dependent terms, and has a zero steady state for all state variables. This modification is equivalent to the addition of integral compensation. This LQR compatible state space can be written in the matrix form $\dot{x} = Ax + Bv$ where the state space is

$$x^T = [E_\theta, \dot{E}_\theta, \dot{q}, E_\psi, \dot{E}_\psi, \dot{r}, \dot{\delta}_E, \dot{\delta}_R, \ddot{\delta}_E, \ddot{\delta}_R]^T$$

the control matrix is $v^T = [\dot{u}_E, \dot{u}_R]^T$, and the system matrices are

$$A = \begin{bmatrix} 0 & 1 & 0 & 0 & 0 & 0 & 0 & 0 & 0 & 0 \\ 0 & 0 & -1 & 0 & 0 & 0 & 0 & 0 & 0 & 0 \\ 0 & 0 & 0 & 0 & 0 & M_r & M_E & 0 & 0 & 0 \\ 0 & 0 & 0 & 1 & 0 & 0 & 0 & 0 & 0 & 0 \\ 0 & 0 & 0 & 0 & -1 & 0 & 0 & 0 & 0 & 0 \\ 0 & 0 & N_q & 0 & 0 & 0 & 0 & N_R & 0 & 0 \\ 0 & 0 & 0 & 0 & 0 & 0 & 0 & 0 & 1 & 0 \\ 0 & 0 & 0 & 0 & 0 & 0 & 0 & 0 & 0 & 1 \\ 0 & 0 & 0 & 0 & 0 & 0 & -H_2 & 0 & -H_1 & 0 \\ 0 & 0 & 0 & 0 & 0 & 0 & 0 & -H_2 & 0 & -H_1 \end{bmatrix} \tag{21a}$$

$$B^T = \begin{bmatrix} 0 & 0 & 0 & 0 & 0 & 0 & 0 & 0 & H_2 & 0 \\ 0 & 0 & 0 & 0 & 0 & 0 & 0 & 0 & 0 & H_2 \end{bmatrix}^T \tag{21b}$$

Integral compensation results from the controller being mechanized with the integral of the state space and with the compensator gains determined via LQR synthesis on Eq. (21). This mechanization provides the proper servo inputs, and the servo input integration cancels the differentiation required to produce the LQR state space. The controllability of MIMO state spaces after the addition of integral compensation must be re-evaluated to ensure that no uncontrollable modes have been introduced.[4] The continuous MIMO pitch- and yaw-angle controller with proportional-integral-derivative (PID) compensation is shown in Fig. 2. The derivative portion of the compensation is mechanized as a gain operating on rate feedback. The implementation of this compensation also includes first-order lag prefilters on the attitude angle commands. This prevents the input of large step commands directly into the controller. The gains on the servo rate states are set to zero because these states are not measured or estimated. The effect of this approximation on stability is discussed in Sec. VII. Although Eq. (21) is shown with a second-order servo model, a first-order approximate model has also been used. Vehicle performance is similar, but the single pole model puts a smaller gain on the servo position feedback and reduces the noise sensitivity of that loop.

A state space for the roll-rate controller can be formed if Eq. (18) is combined with the time derivatives of Eqs. (5), (7), and (8) to produce

$$\begin{bmatrix} \dot{E}_p \\ \ddot{p} \\ \dot{\delta}_A \\ \frac{d}{dt}(\dot{\delta}_A) \end{bmatrix} = \begin{bmatrix} 0 & -1 & 0 & 0 \\ 0 & 0 & L_A & 0 \\ 0 & 0 & 0 & 1 \\ 0 & 0 & -H_2 & -H_1 \end{bmatrix} \begin{bmatrix} E_p \\ \dot{p} \\ \dot{\delta}_A \\ \ddot{\delta}_A \end{bmatrix} + \begin{bmatrix} 0 \\ 0 \\ 0 \\ H_2 \end{bmatrix} \dot{u}_A \tag{22}$$

The block diagram of the resulting proportional-integral continuous roll-rate controller is shown in Fig. 3. The gain on the servo rate state is set to zero. The mechanization of this compensator in software is somewhat different than that shown in that the integrator is pulled through the summing junction. This allows the stable measurement of heading angle from the magnetometer to be used rather than integrated roll-rate gyro output, which usually includes a bias resulting from bias drift since preflight.

The approach taken in the design of the altitude-rate compensator is that of an rpm control loop embedded within the altitude-rate control loop. A state space for the rpm inner loop is obtained by combining Eq. (20) with the time derivatives of Eqs. (7–10) to form

$$\begin{bmatrix} \dot{E}_\Sigma \\ \ddot{\Sigma} \\ \frac{d}{dt}(\ddot{\Sigma}) \\ \ddot{\delta}_T \\ \frac{d}{dt}(\ddot{\delta}_T) \end{bmatrix} = \begin{bmatrix} -1 & 0 & 0 & 0 & 0 \\ 0 & 0 & 1 & 0 & 0 \\ 0 & -H_{E2} & -H_{E1} & (H_{E2}K_E) & 0 \\ 0 & 0 & 0 & 0 & 1 \\ 0 & 0 & 0 & -H_2 & -H_1 \end{bmatrix} \begin{bmatrix} E_\Sigma \\ \dot{\Sigma} \\ \ddot{\Sigma} \\ \dot{\delta}_T \\ \ddot{\delta}_T \end{bmatrix} + \begin{bmatrix} 0 \\ 0 \\ 0 \\ 0 \\ H_2 \end{bmatrix} \dot{u}_T \tag{23}$$

When mechanized with the integral of the state space, a PID compensation structure is produced.

The altitude-rate outer-loop controller design is accomplished by combining the simple dynamics of Eq. (6) with those of a three pole "pseudo-engine" model. This pseudo-engine model is obtained from the three slowest modes of a continuous version of the closed-loop compensator. The input to the pseudo-engine model is taken as the perturbed rpm command output from the altitude-rate controller, whereas the output is approximately the perturbed engine rpm. If Eq. (19) is combined with the time derivatives of Eq. (6) and the third-order pseudo-engine model, an altitude-rate state space is formed as

$$\begin{bmatrix} \dot{E}_{\dot{h}} \\ \frac{d}{dt}(\ddot{h}) \\ \dddot{\Omega} \\ \frac{d}{dt}(\ddot{\Omega}) \\ \frac{d^2}{dt^2}(\ddot{\Omega}) \end{bmatrix} = \begin{bmatrix} 0 & -1 & 0 & 0 & 0 \\ 0 & 0 & [(X_{\text{rpm}}/W)(C_{\text{rpm}})] & 0 & 0 \\ 0 & 0 & 0 & 1 & 0 \\ 0 & 0 & 0 & 0 & 1 \\ 0 & 0 & -H_{\text{rpm3}} & -H_{\text{rpm2}} & -H_{\text{rpm1}} \end{bmatrix} \times \begin{bmatrix} E_{\dot{h}} \\ \ddot{h} \\ \dot{\Omega} \\ \ddot{\Omega} \\ \frac{d}{dt}(\ddot{\Omega}) \end{bmatrix} + \begin{bmatrix} 0 \\ 0 \\ 0 \\ 0 \\ H_{\text{rpm3}} \end{bmatrix} \dot{\Omega}_C \tag{24}$$

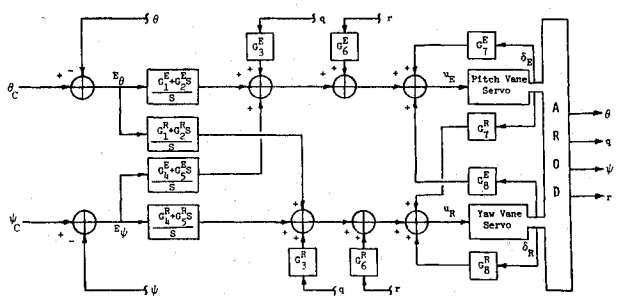

Fig. 2 Pitch- and yaw-angle controller block diagram.

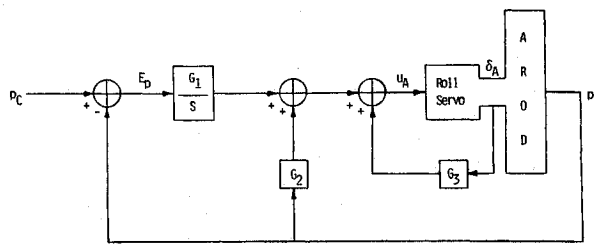

Fig. 3 Roll-rate controller block diagram.

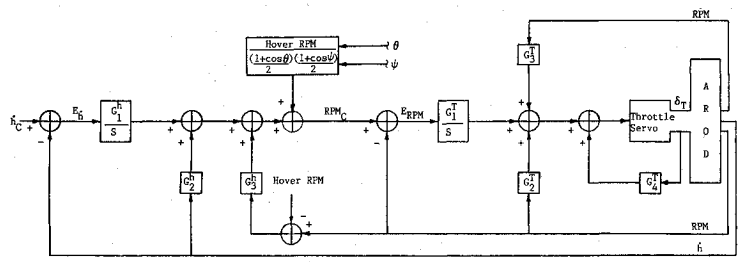

Fig. 4 Altitude-rate controller block diagram.

where the last three equations represent a general third-order pseudo-engine dynamic model. The $\Sigma_C = \Sigma_{\text{hover}} + \Omega_C$ is considered to be a variable here, rather than the constant assumed in Eq. (15). Proportional-integral compensation is the result when the controller is mechanized. The altitude-rate controller with rpm controller inner loop is shown in Fig. 4. The rpm command biasing as a function of vehicle attitude is also depicted. The throttle servo rate state is omitted from the compensator by setting its gain to zero. The rpm-rate state is estimated online from measurements of engine rpm for use by the inner loop. The rpm rate and acceleration states have been determined from field tests to not be essential to the outer loop and those gains are set to zero. The mechanization of the altitude-rate controller is also modified by pulling the integrator through the summing junction and using altitude feedback rather than the integral of the estimated altitude rate.

V. Gain Determination

A. Linear Quadratic Regulator Procedure

The LQR synthesis problem is that of determining the control that minimizes the performance index

$$J = \int (x^T Q x + v^T R v)\, dt \tag{25}$$

where $R > 0$ and $Q \geq 0$, subject to the dynamic constraints

$$\dot{x} = Ax + Bv \tag{26}$$

The solution to this optimization problem is the linear controller

$$v = -(R^{-1}B^T P)x = -Gx \tag{27}$$

where P is the algebraic matrix Riccati equation solution.[5,6] The constant gain matrix G can be determined from any one of several control-system design software packages, which typically allow the input to be in continuous or discrete form. The LQR problem is stated in continuous time, but the gains for AROD are based on determining the discrete form of Eq. (26) and the associated discrete gains for a particular sample rate. There is also a significant computation delay in the AROD software mechanization, and delay compensation must be included. Because the AROD sample rate and computation delay are approximately equal, the discrete state spaces can be augmented with states that represent the controls from the previous iteration. The appended state space is then used as if there is sampling but no delay.

The LQR state weighting matrix for each of the AROD control loops is chosen to satisfy several design criteria. In each case, Q is chosen to provide acceptable transient response behavior and to position the closed-loop system poles such that they are sufficiently smaller than the servo poles. This helps ensure that the servo deflection-rate state gains can be set to zero without seriously compromising system stability. In the case of the MIMO controller, adequate decoupling between the pitch and yaw channels is added to the list of design requirements. System parameter variation sensitivity is also used to evaluate the choice of each Q matrix.

B. Pole Placement Procedure

A pole placement algorithm has been used to determine gains for the altitude- and roll-rate control loops. This algorithm uses the state space models of Sec. IV, except that a two-pole approximation is used for a model of the computation delay. The closed-loop system pole locations are chosen as the result of simulation and field test experience. This procedure places the closed-loop actuator and delay poles at their open-loop positions. Finally, the servo deflection-rate and the delay "rate" gains are set to zero, since these states are not measured or estimated.

C. Preflight Gain Adjustments

A single set of gains is determined by one of the above procedures for each of the AROD controllers. This baseline set of gains is then automatically scaled for optimum performance when the operator inputs the vehicle weight, air temperature, and altitude during preflight operations. These variables are used to calculate the density altitude and hover rpm. The ratios defined by WTRATIO (baseline weight/actual weight) and RPMRATIO (actual hover rpm/baseline hover rpm) are then used to scale the baseline gains to approximately maintain the closed-loop poles of the baseline system. WTRATIO is used to scale those system gains that are a function of the control-vane effectiveness, because the dynamic pressure of the flow over the vanes during hover is a direct function of the vehicle weight. RPMRATIO is used to scale the altitude-rate loop gains that are a function of X_{rpm} and the crossover gains in the MIMO controller that are a function of the hover rpm. Once the baseline gains have been adjusted, the gains are held constant during the entire flight.

VI. Robustness and Singular Value Analysis

The robustness of the AROD pitch/yaw angle controller has been investigated with the use of singular value analysis. Because the servo rate states are not available to provide full state feedback, a measure of the gain and phase margins of the nominal system is required. The procedures of Ref. 7 are applicable, given the singular values of the return difference matrix

$$D(s) = [I + K(s)G_p(s)] \tag{28}$$

where $K(s)$ is the compensator transfer matrix and $G_p(s)$ is the plant transfer matrix given by $G_p(s) = C(sI - A)^{-1}B$, where $K(s)G_p(s) \approx G(sI - A)^{-1}B$.

Singular value analysis is also useful in assessing robustness with respect to particular parameter variations. The matrix of most interest here is the inverse return difference matrix

$$T(s) = I + (K(s)G_p(s))^{-1} \tag{29}$$

The central robustness relationship[8] is that

$$\underline{\sigma}[T(\omega)] > \bar{\sigma}[L(\omega)] \tag{30}$$

for all frequencies ω, where $\underline{\sigma}$ is the smallest and $\bar{\sigma}$ is the largest singular value. $L(\omega)$ is a multiplicative error model,

where the perturbed plant G_p^* is

$$G_p^* = G_p(s)[I + L(s)] \tag{31}$$

An error model for variations in the system parameters, denoted here by ΔA and ΔB, can be derived[4] with $\psi(s) = (sI - A)^{-1}$ as

$$L(s) = G_p^{-1} C\psi[\Delta B + \Delta A(I + \psi\Delta A)^{-1}\psi B - \Delta A(I + \psi\Delta A)^{-1}\psi\Delta B] \tag{32}$$

If Eq. (30) is satisfied, then stability is guaranteed. This condition is conservative, and failure of this test does not necessarily imply instability. These procedures are applied to the MIMO controller in the next section.

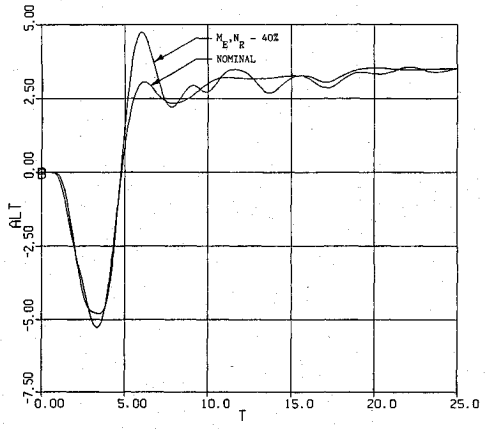

Fig. 5 Altitude vs time.

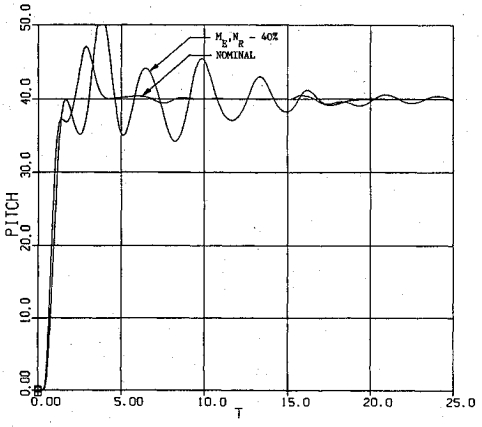

Fig. 6 Pitch angle vs time.

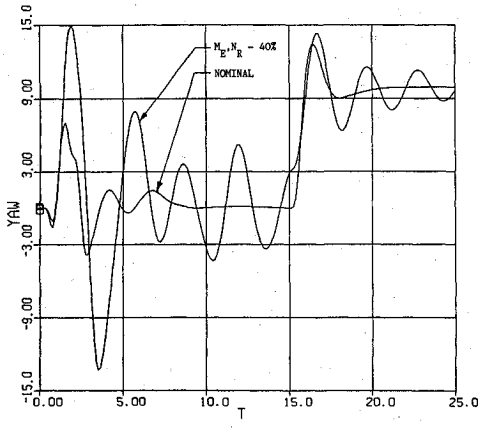

Fig. 7 Yaw angle vs time.

VII. System Performance

The performance of the AROD control system has been evaluated by time response behavior against a six degree-of-freedom, nonlinear, dynamic simulation that includes wind-tunnel forces and moments, by a singular value analysis, and by gimbal fixture and limited flight tests in the field.

Some representative simulated transient responses are given in Figs. 5–9 for an AROD with a c.g. 4.5 in. aft of the duct leading edge. The vehicle is initially commanded to pitch over 40 deg from a hover state with a zero climb rate. This is a rather radical change in commanded attitude that is intended to demonstrate control-system robustness to unmodeled dynamics. At 15 s, a yaw command of 10 deg is also applied. This command sequence is consistent with a skid-to-turn maneuver. The alternative and probably more efficient turning technique is to return to hover, roll to a new heading, and then pitch over into horizontal flight. The use of heading angle as a roll-angle feedback is not consistent with the skid-to-turn portion of this command sequence, however, and is replaced with an integrated roll rate for purposes of these plots. Figure 5 shows the altitude vs time plot. The steady-state altitude offset here is due to the rpm command bias applied as a function of vehicle attitude. There is an altitude loss of about 5 ft during the pitch maneuver. The altitude loss transient would be smaller for a more reasonable change in the commanded attitude. A velocity of about 48 ft/s is attained in steady level flight at 40 deg of pitch angle. Pitch and yaw angles are plotted, respectively, in Figs. 6 and 7. The gyroscopic coupling between the two channels is evident from the yaw angle transient when the pitch step command is executed. The time history of the pitch- and yaw-vane deflections are given in Figs. 8 and 9. The pitch-vane trim deflection in steady state is required to counter the aerodynamic pitch-up moments, whereas the yaw-vane trim deflection is required to take out the propellor "P factor" (differential lift on the

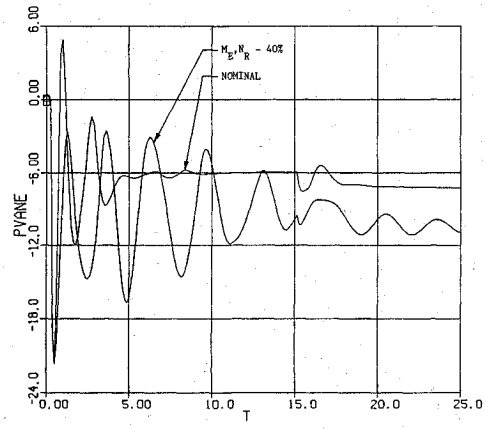

Fig. 8 Pitch-vane deflection vs time.

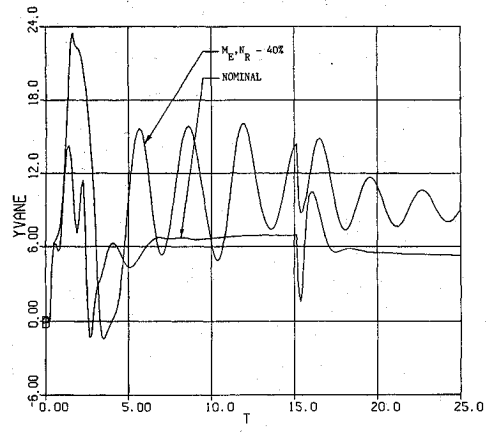

Fig. 9 Yaw-vane deflection vs time.

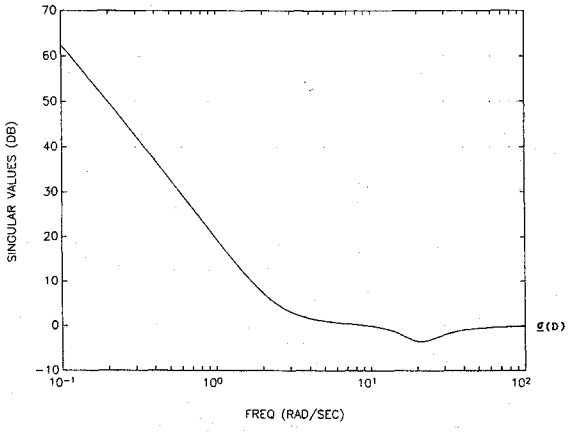

Fig. 10 Minimum singular value of the return difference matrix for the pitch/yaw controller.

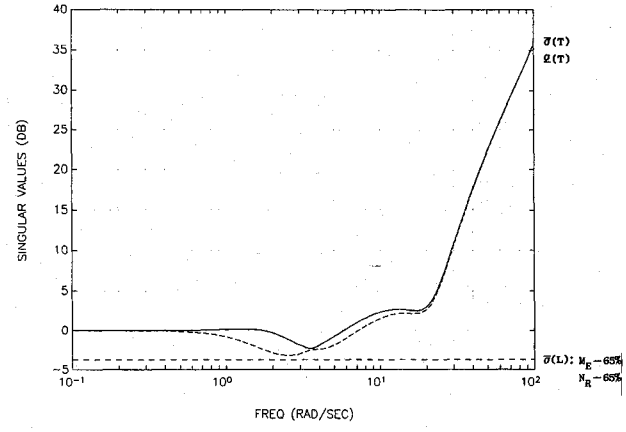

Fig. 11 Singular values of pitch/yaw-vane effectiveness error model vs inverse return difference matrix.

fixed pitch propellor at nonzero angles of attack). Superimposed on the nominal response is a response that corresponds to a 40% reduction in the effectiveness of the control surfaces. A 50% reduction in effectiveness is possible without instability, but the response is poorly damped.

A plot of the minimum singular value of the return difference matrix [Eq. (28)] for the MIMO pitch- and yaw-angle controller is given in Fig. 10. This plot indicates a minimum of −3.5 dB. Since a full feedback LQR design would have a minimum of 0.0 dB,[9-11] there is a stability margin penalty due to the lack of full state feedback. The minimum gain and phase margins can be determined from Ref. 7 as a gain margin of (−4.3, +10) dB and a phase margin of ±40 deg. These minimums occur at the servo natural frequency, and the control-system bandwidth is well below this frequency. Figure 11 shows the singular values for the inverse return difference matrix [Eq. (29)] for the nominal MIMO system, plotted against the error model [Eq. (32)] for variations in the effectiveness coefficients M_E and N_R. This plot indicates that perturbations of ±65% are possible without instability. This plot does not, however, include effects such as dynamical nonlinearities, aerodynamics, sampling, and computation delays.

System data and gains for the AROD vehicle are given in Table 2. Performance index weighting matrices and the open- and closed-loop system eigenvalues are shown in Table 3. Average system parameters have been used to determine gains for field testing because of the resulting gain symmetry, which expedites insertion and verification of test gains into the software. This vehicle was first tested in a gimbal test fixture that allowed simultaneous pitch, yaw, and roll movements. Data from these tests confirmed the previously measured system parameters and provided a preliminary validation of the control system and software. The limited flight testing program included free flights, free flights over a net, and flights with the vehicle on a tether with three different AROD designs. This portion of the development program extended from December 1986 to April 1988. Flights were conducted in

Table 2 Control-system parameters and gains

System parameters
Control-vane servo model: $f_n = 20$ rad/s, £ = 0.50
Throttle servo model: $f_n = 20$ rad/s, £ = 0.60
Engine model: $f_n = 5.0$ rad/s, £ = 1.0, $K_E = 900.0$ rad/s/rad
Propellor effectiveness: $X_{\text{rpm}} = 0.2387$ lb$_f$/rad/s
Hover rpm: 6000 rpm
Mass properties:
$W = 75$ lb$_m$, $I_p = 41.62$ lb$_m$ in.^{2}
$A = 6563.0$ lb$_m$ in.^{2}, $B = 16145.0$ lb$_m$ in.^{2}, $C = 14716.0$ lb$_m$ in.^{2}
Control-vane effectiveness coefficients:
$M_E = -11.19$ rad/s^2, $N_R = -12.28$ rad/s^2
$L_A = -19.54$ rad/s^2
Gyroscopic coupling coefficients: $M_r = -1.62$, $N_q = 1.78$
Sample rate: 0.12 s
Computation delay: 0.12 s
Discrete control gains
Altitude rate (outer loop)
6.7803 −16.931 −0.5825 1.0e − 20
Rpm (inner loop)
0.0035997 −0.0014399 −0.00014399 0.012959 0.028078
Roll rate
−0.2589 0.2097 −0.2047 −0.4567
Pitch angle
(using average parameters: $M_E = N_R = -11.74$, $M_r = -1.70$, $N_q = 1.70$; single pole (20 rad/s) servo model)
−1.3087 −1.4050 0.6585 −0.4244 −0.4556 −0.1062 −0.3510 0.0452 −0.7409 0.0649
Yaw angle (using average parameters)
0.4244 0.4556 0.1062 −1.3087 −1.4050 0.6585 −0.0452 −0.3510 −0.0649 −0.7409

Table 3 LQR weighting matrices and system eigenvalues

LQR performance index weighting matrices

$$Q_{\text{Roll}} = \begin{bmatrix} 0.2 & 0.0 & 0.0 & 0.0 & 0.0 \\ 0.0 & 0.0 & 0.0 & 0.0 & 0.0 \\ 0.0 & 0.0 & 0.0 & 0.0 & 0.0 \\ 0.0 & 0.0 & 0.0 & 0.0 & 0.0 \\ 0.0 & 0.0 & 0.0 & 0.0 & 0.0 \end{bmatrix}$$

$R_{\text{Roll}} = 1.$

$$Q_{\text{MIMO}} = \begin{bmatrix} 4.1 & 0.0 & 0.0 & 0.0 & 0.0 & 0.0 & 0.0 & 0.0 & 0.0 & 0.0 \\ 0.0 & 0.54 & 0.0 & 0.0 & 0.0 & 0.0 & 0.0 & 0.0 & 0.0 & 0.0 \\ 0.0 & 0.0 & 0.043 & 0.0 & 0.0 & 0.0 & 0.0 & 0.0 & 0.0 & 0.0 \\ 0.0 & 0.0 & 0.0 & 4.1 & 0.0 & 0.0 & 0.0 & 0.0 & 0.0 & 0.0 \\ 0.0 & 0.0 & 0.0 & 0.0 & 0.54 & 0.0 & 0.0 & 0.0 & 0.0 & 0.0 \\ 0.0 & 0.0 & 0.0 & 0.0 & 0.0 & 0.043 & 0.0 & 0.0 & 0.0 & 0.0 \\ 0.0 & 0.0 & 0.0 & 0.0 & 0.0 & 0.0 & 0.0 & 0.0 & 0.0 & 0.0 \\ 0.0 & 0.0 & 0.0 & 0.0 & 0.0 & 0.0 & 0.0 & 0.0 & 0.0 & 0.0 \\ 0.0 & 0.0 & 0.0 & 0.0 & 0.0 & 0.0 & 0.0 & 0.0 & 0.0 & 0.0 \\ 0.0 & 0.0 & 0.0 & 0.0 & 0.0 & 0.0 & 0.0 & 0.0 & 0.0 & 0.0 \end{bmatrix}$$

$R_{\text{MIMO}} = I_2$

S-plane system eigenvalues

Open-loop rpm eigenvalues:	0.00
	$0.00 \pm 0.00i$
	$-12.00 \pm 16.00i$
Closed-loop rpm eigenvalues:	-2.50
(assumes full state feedback)	$-5.00 \pm 0.00i$
	$-12.00 \pm 16.00i$
Open-loop altitude-rate eigenvalues:	$0.00 \pm 0.00i$
	-2.50
	$-5.00 \pm 0.00i$
Closed-loop altitude-rate eigenvalues:	$-0.5892 \pm 0.5892i$
(assumes full state feedback)	-2.50
	$-5.00 \pm 0.00i$
Open-loop roll-rate eigenvalues:	$0.00 \pm 0.00i$
	$-10.00 \pm 17.32i$
Closed-loop roll-rate eigenvalues:	$-1.77 \pm 1.77i$
(assumes full state feedback)	$-10.00 \pm 17.32i$
Open-loop MIMO eigenvalues:	$0.00 \pm 0.00i$
	$0.00 \pm 0.00i$
	$0.00 \pm 1.70i$
	$-20.00 \pm 0.00i$
Closed-loop MIMO eigenvalues:	$-1.75 \pm 1.77i$
(assumes full state feedback)	$-2.46 \pm 0.53i$
	$-2.41 \pm 2.98i$
	$-19.81 \pm 0.04i$

Albuquerque, New Mexico (6000-ft altitude) and at Camp Pendleton, CA (300-ft Altitude). These flights were conducted primarily for hardware and software development, operator training, and official demonstrations. Ground effect has been a complicating factor for takeoffs and landings. Full power takeoffs and ground crew assisted landings (via a handling ring not shown in Fig. 1) have provided simple and efficient solutions. All flights to date have been conducted within 15 deg of hover. Qualitatively speaking, the control system has performed well and in a manner consistent with simulated results. A comprehensive test and evaluation program, which would provide supporting flight test data, has not yet materialized.

VIII. Conclusions

The control system for the Marine Corps Airborne Remotely Operated Device unmanned air vehicle has been discussed. A control design based on a simplified linear dynamic model has been shown via simulation to be capable of meeting all mission objectives with adequate performance. The primary design complication has been the gyroscopic coupling between the pitch and yaw axes. A simulation study has shown that a linear-quadratic-regulator synthesis procedure produces a compensator with better decoupling performance than that obtained via a classical design approach. The difficulty of the decoupling problem is related to the selection of control servos with a relatively low natural frequency. A limited flight test program has demonstrated that the control system performs well for near hover flight. A comprehensive flight test program would, however, be required to fully validate the control-system design.

References

[1]Arlowe, H. D., "Airborne Remote Operated Device," *Proceedings of the Fifteenth Annual Technical Symposium and Exhibition of the Association for Unmanned Vehicle Systems*, Association for Unmanned Vehicle Systems, Washington, DC, June 1988.

[2]Weir, R. J., "Aerodynamic Design Considerations for a Free-Flying Ducted Propellor," *Proceedings of the 1988 Atmospheric Flight Mechanics Conference*, AIAA, Washington, DC, Aug. 1988, pp. 720–731.

[3]Athans, M., "On the Design of P-I-D Controllers Using Optimal Linear Regulator Theory," *Automatica*, Vol. 7, Sept. 1971, pp. 643–647.

[4]Speyer, J. L., White, J. E., Douglas, R., and Hull, D. G., "Multi-Input/Multi-Output Controller Design for Longitudinal Decoupled Aircraft Motion," *Journal of Guidance, Control, and Dynamics*, Vol. 7, No. 6, 1984, pp. 695–702.

[5]Brockett, R., *Finite Dimensional Linear Systems*, Wiley, New York, 1970.

[6]Bryson, A., and Ho, Y.-C., *Applied Optimal Control*, Blaisdell, Waltham, MA, 1969.

[7]Mukhopadhyay, V., and Newsom, J., "A Multiloop System Stability Margin Steady Using Matrix Singular Valves," *Journal of Guidance, Control, and Dynamics*, Vol. 7, No. 5, 1984, pp. 582–587.

[8]Doyle, J., and Stein, G., "Multivariable Feedback Design: Concepts for a Classical/Modern Synthesis," *IEEE Transactions on Automatic Control*, Vol. AC-26, Feb. 1981, pp. 4–16.

[9]Sain, M., (ed.), "Special Issue on Multivariable Control," *IEEE Transactions on Automatic Control*, Vol. AC-26, Feb. 1981.

[10]Safonov, M. G., and Athans, M., "Gain and Phase Margin for Multiloop LQG Regulators," *IEEE Transactions on Automatic Control*, Vol. AC-22, April 1977, pp. 173–179.

[11]Lehtomaki, N., Sandell, N., and Athans, M., "Robustness Results in Linear-Quadratic Gaussian Based Multivariable Control Design," *IEEE Transactions on Automatic Control*, Vol. AC-26, Feb. 1981, pp. 75–92.